Cancer Research

Inhibition of Dipeptidyl Peptidase-4 Accelerates Epithelial–Mesenchymal Transition and Breast Cancer Metastasis via the CXCL12/CXCR4/mTOR Axis

Fan Yang[1], Yuta Takagaki[1], Yasuo Yoshitomi[2], Takayuki Ikeda[2], Jinpeng Li[1], Munehiro Kitada[1,3], Asako Kumagai[1], Emi Kawakita[1], Sen Shi[1], Keizo Kanasaki[1,3], and Daisuke Koya[1,3]

Abstract

Dipeptidyl peptidase (DPP)-4 is a multifunctional glycoprotein involved in various biological and pathologic processes. DPP-4 has been widely recognized as a therapeutic target for type 2 diabetes mellitus but is also implicated in the development of human malignancies. Here, we show that inhibition of DPP-4 accelerates breast cancer metastasis via induction of CXCL12/CXCR4, which activates mTOR to promote epithelial–mesenchymal transition (EMT). In cultured cells, DPP-4 knockdown induced EMT and cell migration. Treatment with the DPP-4 inhibitor KR62436 (KR) promoted primary tumor growth and lung metastasis in a 4T1 tumor allograft mouse model; DPP-4 knockdown in 4T1 cells displayed similar phenotypes *in vivo* and *in vitro*. KR treatment enhanced the levels of CXCL12/CXCR4 and phosphorylated mTOR, which were associated with the induction of EMT in metastatic cancer cells. KR-induced EMT in cancer cells was inhibited by treatment with the CXCR4 inhibitor AMD3100 or the mTOR inhibitor rapamycin, and AMD3100 suppressed KR-induced metastasis *in vivo*. Our findings suggest that DPP-4 plays a significant role in cancer biology and that inhibition of DPP-4 promotes cancer metastasis via induction of the CXCL12/CXCR4/mTOR/EMT axis.

Significance: These findings reveal that inhibition of DPP-4 increases the metastatic potential of breast cancer. This is especially important given the potential use of DPP-4 inhibition as a therapeutic strategy for type 2 diabetes.

Introduction

Invasion and metastasis are the final common steps in the progression of any type of human malignancy (1). Breast cancer is the most commonly diagnosed cancer in women worldwide (2). Most breast cancer–related deaths are caused by metastasis rather than the primary tumor itself (3). However, the molecular mechanisms that underlie breast cancer metastasis have not been completely elucidated.

Epithelial–mesenchymal transition (EMT) is a molecular program whereby epithelial cells undergo reprogramming from a polarized, differentiated phenotype with numerous cell–cell junctions to a mesenchymal phenotype (4). During EMT, cancer cells lose their cell–cell adhesion properties and acquire invasive and migratory properties (5). EMT has shown to be associated with increased potential for cancer cell motility, metastasis, and chemotherapy resistance (6).

Dipeptidyl peptidase (DPP)-4, a membrane glycoprotein, has been shown to affect multiple biological processes, such as cell differentiation, adhesion, immunomodulation, and apoptosis (7). Accumulating evidence indicates that DPP-4 plays an important role in cancer progression (8–10). A recent study confirmed that a DPP-4 inhibitor does not increase tumor incidence but may promote the metastasis of multiple cancer cell lines (11). DPP-4 catalytically regulates the activity of biopeptides by proteolytically cleaving a number of peptides, cytokines, and chemokines (12). C-X-C motif chemokine 12 (CXCL12), also known as stromal cell–derived factor 1 (SDF1), is a confirmed substrate of DPP-4 (13). CXCL12 binds to C-X-C receptor 4 (CXCR4) and CXCR7 and thus regulates tumor growth and metastasis (14). In breast cancer, the CXCL12/CXCR4 axis plays an important role in directing the metastasis of $CXCR4^+$ cancer cells to organs that express high CXCL12 levels, such as the lungs, bone marrow, and lymph nodes (15). Therefore, an increase in CXCL12 levels in response to DPP-4 inhibitor treatment could be relevant to the metastasis of CXCR4-positive cancer (16).

mTOR, a major effector of the PI3K/Akt pathway, is associated with mRNA translation, glucose metabolism, and autophagy and is involved in malignant transformation (17). mTOR exists in two complexes: mTORC1 (containing mTOR, Raptor, etc.) and mTORC2 (containing mTOR, Rictor, etc.). mTORC1 is somewhat

[1]Department of Diabetology & Endocrinology, Kanazawa Medical University, Uchinada, Ishikawa, Japan. [2]Department of Biochemistry, Kanazawa Medical University, Uchinada, Ishikawa, Japan. [3]Division of Anticipatory Molecular Food Science and Technology, Medical Research Institute, Kanazawa Medical University, Uchinada, Ishikawa, Japan.

Note: Supplementary data for this article are available at Cancer Research Online (http://cancerres.aacrjournals.org/).

Corresponding Authors: Keizo Kanasaki, Kanazawa Medical University, 1-1 Daigaku, Uchinada, Ishikawa 920-0293, Japan. Phone: 817-6286-2211, ext. 3305; Fax: 817-6286-6927; E-mail: kkanasak@kanazawa-med.ac.jp; and Daisuke Koya, koya0516@kanazawa-med.ac.jp

doi: 10.1158/0008-5472.CAN-18-0620

sensitive to rapamycin treatment, whereas mTORC2 is believed to be rapamycin insensitive (18). A recent finding implicated mTORC1 and mTORC2 as key regulators of EMT. Knockdown of mTORC1 and mTORC2 induced mesenchymal–epithelial transition (MET), and inhibition of mTOR signaling suppressed cancer cell migration and invasion (19). Furthermore, cross-talk between the mTOR pathway and CXCL12/CXCR4 axis suggests that mTORC1 knockdown is sufficient to decrease CXCR4-mediated migration, and inhibition of mTORC1 by rapamycin decreases primary tumor growth and CXCR4-mediated lymph node metastasis (20).

Here, we hypothesize that activation of the CXCL12/CXCR4/mTOR signaling pathway in response to DPP-4 suppression plays a key role in the regulation of EMT and metastasis in breast cancer.

Materials and Methods

Reagents and antibodies

KR62436 hydrate (KR, K4264), AMD3100 (A5602), rapamycin (R8781), and recombinant mouse CXCL12α (SRP4388) were purchased from Sigma. Recombinant TGFβ1 was purchased from PeproTech (100-21). The following antibodies were purchased from Abcam: rabbit polyclonal anti-αSMA (1:1,000, ab5694, RRID: AB_2223021), mouse monoclonal anti-vimentin (1:2,000, ab8978, RRID: AB_306907), rabbit polyclonal anti-TGFβR2 (1:1,000, ab61213, RRID: AB_945809), goat polyclonal anti-CXCR4 (1:1,000, ab1670, RRID: AB_302470), and rabbit polyclonal anti-CXCL12 (1:1,000, ab18919, RRID: AB_444705). The rabbit polyclonal anti-Smad3 (1:1,000, CST9513, RRID: AB_2286450), rabbit polyclonal anti-phospho-mTOR (1:1,000, 2974, RRID: AB_2262884), rabbit polyclonal anti-mTOR (1:1,000, 2983, RRID: AB_2105622), and rabbit polyclonal anti-GFP (1:1,000, 2555, RRID: AB_ 10692764) antibodies were purchased from Cell Signaling Technology. The mouse monoclonal anti–β-actin (1:10,000, A2228, RRID: AB_476697), rabbit anti-TGFβR1 (1:500, SAB4502958, RRID: AB_10746304), and goat polyclonal anti-DPP-4 (1:500, SAB2500328, RRID: AB_10603974) antibodies were obtained from Sigma. A rat monoclonal anti–E-cadherin antibody was purchased from GeneTex (1:2,000, GTX11512, RRID: AB_381324). A rabbit polyclonal anti-phospho-Smad3 (s423 and s425) antibody (1:1,000, 600-401-919, RRID: AB_2192878) was purchased from Rockland Immunochemicals. The neutralizing TGFβ (1, 2, 3) antibody (MAB1835, RRID: AB_357931), recombinant mouse DPP-4 (954-SE) and neutralizing CXCL12 antibody (MAB310, RRID: AB_2276927) was purchased from R&D Systems. Fluorescein (FITC)-conjugated anti-rat IgG (1:200,112-095-003, RRID: AB_2338189) and Cy-conjugated anti-rabbit IgG (1:200, 111-166-047, RRID: AB_2338010) secondary antibodies were obtained from Jackson Immuno Research. Mounting medium containing DAPI (H-1200, RRID: AB_2336790) was obtained from Vector Laboratories.

Cell culture and treatment

The experimental cell lines were obtained from ATCC. Some *in vitro* experiments were performed using cell lines obtained from the ATCC and cryopreserved for more than 6 months. In addition, some results were confirmed using cell lines obtained from the ATCC within 6 months. Identities of the cells were confirmed by following methods: COI assay for human MCF 10A mammary epithelial cells (CRL-10317, RRID: CVCL_0598), human MCF7 breast cancer cells (HTB-22, RRID: CVCL_0031), human MDA-MB-231 breast cancer cells (HTB-26, RRID: CVCL_0062), and mouse 4T1 breast cancer cells (CRL-2539, RRID: CVCL_0125; GFP-expressing cells), and short tandem repeat analysis for MCF7 cells and MCF10A cells. All cell lines were grown at 37°C in a 5% CO_2 atmosphere, used for 10 passages after reviving from the frozen vials and regularly stained with DAPI (Vector Labs) to test for *Mycoplasma* contamination every 3 months. Also, we confirmed negative test for *Mycoplasma* by PCR (test no.18Q397, 21st Nov. 2018, ICLAS Monitoring Center, Japan). MCF10A cells were cultured in MEBM supplemented with MEGM (BPE, hEGM, insulin, hydrocortisone, and GA-1000; Lonza). MCF7 cells (HTB-22, RRID: CVCL_0031) were cultured in ATCC-formulated Eagle minimum essential medium with 0.01 mg/mL human recombinant insulin and 10% (final concentration) FBS. MDA-MB-231 cells were cultured in ATCC-formulated Leibovitz L-15 medium with 10% FBS. A mixture of CO_2 and air is detrimental to cells when using this medium for cultivation. 4T1 cells were cultured in RPMI1640 medium with 10% FBS. When the cells reached 70%–80% confluence, KR (50 μmol/L), AMD3100 (30 μmol/L), TGFβ1 (5 ng/mL), neutralizing TGFβ (1, 2, 3) antibody (1.0 μg/mL), rapamycin (1 μmol/L), recombinant mouse DPP-4 (1 μg/mL), recombinant mouse CXCL12α (0.2 μg/mL), or neutralizing CXCL12 antibody (200 μg/mL) was added to the experimental medium.

Transfection experiments

4T1 cells were transfected with siRNA (100 nmol/L) targeting mouse DPP-4 (5′-CCGUGCCAAUAGUUCUGCU-3′; AM16704, Invitrogen). MCF 10A, MCF7, and MDA-MB-231 cells were transfected with siRNA (100 nmol/L) targeting human DPP-4 (5′-GGAAUGCCAAGGAGGAAGGAAUCUUU-3′; HSS102892, Invitrogen). The transfection reagent Lipofectamine 2000 (Invitrogen) was used according to the manufacturer's instructions. Cells were incubated with Lipofectamine 2000 and siRNA in serum-free medium for 6 hours. Then, the medium was replaced with experimental medium. For DPP-4 siRNA transfections, 4T1 cells were treated with or without TGFβ1 (1.0 g/mL) for 48 hours. The mouse DPP-4 shRNA vectors were constructed in the pSIH vector (System Biosciences) using synthetic oligonucleotides against mouse DPP-4 antisense sequences (shDPP-4-1: 5′-TAGAAGGAGTATTCAATGAGC-3′ or shDPP-4-2, 5′-AATAGT-CAGCTA-GTGAATACG-3′ or shDPP-4-3: 5′-ATAGTAGAGGA-TATTTCTTGG -3′) with loop 5′-CTCGAG-3′. Lentivirus particles were propagated in HEK293TN cells (System Biosciences) following transfection with the pM2.G envelope vector and the packaging psPAX2 vector (deposited by Didier Trono, Laboratory of Virology and Genetics, Ecole Polytechnique Federale de Lausanne, Switzerland; Addgene plasmid #12259 and #12260, respectively, Addgene). Supernatants from 48-hour cultures were collected, and then lentiviral particles were concentrated using PEG-it solution (System Biosciences). Lentivirus transduction efficiencies were then determined according to numbers of GFP-positive 4T1 cells at 48 hours posttransduction. Lentivirus experiments were approved by the Kanazawa Medical University Safety Committee for Recombinant DNA experiment (protocol number: 2018-11).

Mouse breast cancer models

Female BALB/c mice (8 weeks old; CLEA Japan, Inc., Japan, RRID: MGI: 3586693) were anesthetized. Incisions (0.5 cm each)

were made on the mouse abdomen between the 1st and 2nd sets of nipples counting from the hind leg of the animal. Cultured 4T1 cells (5×10^5 cells in 20 μL of PBS) were injected into the mammary fat pad of each mouse using a Hamilton syringe fitted with a 25G needle. At 20 days posttumor cell injection, the primary tumor measured approximately 500 mm^3. At this point, the mouse breast cancer model was treated with PBS orally, KR (0.02 mg/g/day, orally), AMD3100 (0.0075 mg/g/day i.p), or KR and AMD3100. Seven days after initiating treatment, the mice were sacrificed, and the primary tumor tissues and lungs were removed. The shRNA-control or shRNA-DPP-4–transduced 4T1 cells were injected into the mammary fat pad of each mouse. Twenty-seven days after tumor cells injection, the mice were sacrificed, and the primary tumors and lungs were analyzed. The experiments described herein were conducted in accordance with the animal protocols of Kanazawa Medical University (protocol numbers 2014-89, 2013-114, and 2014-101, lentivirus shRNA *in vivo* experiment protocol number 2018-17).

Western blot analysis

Proteins were harvested using RIPA lysis buffer containing phenylmethylsulfonylfluoride, protease inhibitor cocktail, and sodium orthovanadate (Santa Cruz Biotechnology). Protein lysates were boiled in SDS sample buffer at 100°C for 6 minutes, separated on SDS-polyacrylamide gels, and then transferred onto polyvinylidene difluoride membranes (Pall Corporation) using the semidry method. After blocking, the membranes were incubated overnight with primary antibodies at 4°C, followed by incubation with the corresponding peroxidase-conjugated secondary antibody for 1 hour at room temperature. The blots were developed with an enhanced Chemiluminescence Detection System (Pierce Biotechnology) and visualized using an Image-Quant LAS 400 Camera System (GE Healthcare Life Sciences).

Immunofluorescence analysis

Treated 4T1 cells were cultured on 8-well culture slides (354630, BioCoat) for 48 hours. The cells were then fixed with 100% methanol for 10 minutes at −20°C and with acetone for 1 minute at −20°C. After being blocked with 2% BSA/PBS for 30 minutes at room temperature, the cells were incubated with primary antibody for 1 hour, washed with PBS, and incubated with the corresponding secondary antibody for 30 minutes. The cells were then extensively washed three times with PBS and mounted with mounting medium containing DAPI. The images were analyzed by confocal microscopy (LSM710, Carl Zeiss).

Hematoxylin and eosin staining and Opal triple immunofluorescence staining

Paraffin slides were deparaffinized in 2 changes of xylene for 5 minutes each and transferred to 100%, 95%, and 70% alcohol for 3 minutes each. Then, the slides were stained with hematoxylin and eosin (H&E) solution. After being incubated in 3% H_2O_2 solution for 10 minutes to block endogenous peroxidase activity, the slides were incubated in 300 mL of 10 mmol/L citrate buffer (pH 6.0) at 100°C for 1 hour. The slides were incubated with primary antibody for 1 hour, washed with TBST, and incubated with the corresponding secondary antibody for 30 minutes. Then, the slides were incubated with reactive fluorophores (Opal 520, Opal 570, and Opal 670; Opal 4-Color Automation IHC Kit, NEL801001KT, Perkin Elmer). The proteins were stained sequentially. Finally, the slides were mounted with spectral DAPI, and the images were analyzed by confocal microscopy (LSM710, Carl Zeiss).

Immunohistochemistry analysis

Paraffin slides were deparaffinized in 2 changes of xylene for 5 minutes each and transferred to 100%, 95%, and 70% alcohol for 3 minutes each. After being incubated in 3% H_2O_2 at room temperature for 10 minutes to block endogenous peroxidase activity, the slides were incubated in 300 mL of 10 mmol/L citrate buffer (pH 6.0) at 100°C for 1 hour. The slides were then incubated with primary antibody for 1 hour, washed with PBS, and incubated with the corresponding secondary antibody for 30 minutes. The slides were incubated with 100 μL of DAB substrate solution (SK-4100, Vector Laboratories). After being stained with hematoxylin for 2 minutes, the tissue slides were dehydrated through 4 changes of alcohol (95%, 95%, 100%, and 100%) for 5 minutes each and hyalinized in 3 changes of xylene. The images were analyzed by the NanoZoomer Digital Pathology System.

Transwell migration assay

Matrigel (BD, No. 356234) was thawed on ice overnight at 4°C. Cell culture inserts (0264, BD Falcon) were coated with Matrigel and incubated at 37°C for 1 hour. MCF 10A, MCF7, MDA-MB-231, and 4T1 cells were placed in the top chamber of a cell culture insert with serum-free medium, and complete media were added to the bottom chambers of the inserts in 6-well plates. Following treatment with control siRNA, DPP-4 siRNA, KR, AMD3100 or KR, and AMD3100 for 24 hours, the cells that migrated through the membrane were stained with hematoxylin and counted. Migration was analyzed by microscopy (Carl Zeiss Microscopy). Images of 6 different fields of view were obtained at 200× magnification, and the results were quantified.

Morphologic evaluation

MCF 10A, MCF7, MDA-MB-231, and 4T1 cells were incubated in 6-well plates (cell culture–treated multidishes; 140675, Thermo Fisher Scientific) and treated with control siRNA or DPP-4 siRNA. Morphologic changes were analyzed by microscopy (Carl Zeiss Microscopy).

Bouin buffer staining

To identify metastasis on the lung surface, lung specimens were perfused with 10% formaldehyde and then fixed in the same solution after dissection. Next, the lungs were placed in Bouin buffer (10% formaldehyde: 0.9% picric acid: 5% acetic acid = 15:5:1) for at least 24 hours after dehydration in 100% ethanol. Surface lung metastasis was quantitated by counting the number of metastatic nodules.

DPP-4 activity fluorometric assay

Primary tumor, lung, and plasma samples were homogenized in 4 volumes of DPP-4 Assay Buffer (DPP-4 Activity Fluorometric Assay Kit, K779-100, BioVision) and centrifuged at 13,000 × *g* for 10 minutes to remove insoluble material. Plasma samples were directly diluted in DPP-4 Assay Buffer. The samples were adjusted to a final volume of 50 μL in a 96-well plate using DPP-4 Assay Buffer. Reaction mix (40 μL) was added to each well, and the 96-well plate containing samples was incubated at 37°C for 30 minutes. DPP-4 activity was analyzed by Fluoroskan Ascent (Thermo Fisher Scientific).

ELISA

A mouse CXCL12 ELISA kit was used to detect CXCL12 (DY460, R&D Systems). CXCL12 was quantitated according to the manufacturer's instructions, and the results are presented in ng/mL.

MTT assay

In vitro MTT-based Assay Kit (TOX-1, Sigma) was used for proliferation detection. Cells were incubated with reconstituted MTT in an amount equal to 10% of the culture medium volume for 2 hours. MTT assay was performed following the manufacturer's protocol. The absorbance was measured by spectrophotometric assay at a wavelength of 570 nm.

RNA isolation and qPCR

Total RNA was isolated from small pieces of primary tumor tissue and 4T1 cells using a Qiagen RNeasy Mini Kit (Qiagen). Complementary DNA (cDNA) was generated by using SuperScript (Invitrogen). qPCR was performed in a 7900HT Fast Real-time PCR System (Life Technologies) using SYBR Green (miScript SYBR Green PCR Kit, Qiagen) and 3 ng of cDNA, and the data were quantified using the delta–delta threshold cycle (C_t) method ($\Delta\Delta C_t$). All experiments were performed in triplicate, and β-actin was utilized as an internal control.

Statistical analysis

The data are presented as the mean ± SEM. One-way ANOVA followed by Tukey multiple comparison test was used to determine significance, which was defined as $P < 0.05$, unless otherwise noted. GraphPad Prism software (ver. 5.0f; RRID: SCR_002798) was used for the statistical analysis.

Results

DPP-4 suppression was associated with EMT induction

To study the effects of DPP-4 inhibition on EMT, we utilized siRNA-mediated knockdown of DPP-4. Western blot analysis revealed that DPP-4 knockdown decreased expression of the epithelial marker E-cadherin and increased expression of the mesenchymal markers αSMA and vimentin in the human MCF 10A normal mammary epithelial cell line and in the MCF7 and MDA-MB-231 cancer cell lines (Fig. 1A), suggesting that EMT is induced by DPP-4 suppression. Interestingly, the induction of EMT was significantly greater in metastatic cancer cells (MDA-MB-231) than in other cells (Fig. 1A).

We treated the mouse 4T1 breast cancer cell line with an EMT inducer, TGFβ1, and found that DPP-4 knockdown augmented EMT in the presence of TGFβ1 (Fig. 1B). There was no significant morphologic alteration in DPP-4-knockdown MCF 10A cells, but DPP-4-knockdown MCF7 or MDA-MB-231 cells adopted an elongated or spindle shape compared with control siRNA–transfected cells (Fig. 1C). Transwell assays revealed that DPP-4 inhibition accelerated cell migration (Fig. 1D).

DPP-4 inhibition promoted EMT and metastasis in orthotopic xenograft breast cancer models

To determine the pathologic significance of DPP-4 inhibition *in vivo*, we analyzed 4T1 tumor–bearing female BALB/c mice. Primary tumors and lungs were collected from these mice after 7 days of treatment with PBS or KR, a DPP-4 inhibitor. KR-treated tumor-bearing mice exhibited increased primary tumor growth and weight compared with control tumor-bearing mice (Fig. 2A). The lungs of KR-treated mice had significantly more visible metastatic nodules detected by Bouin buffer staining (Fig. 2B). We also analyzed stable shRNA-DPP-4–transduced 4T1 cells and confirmed that shRNA-DPP-4–transduced 4T1 cells displayed same phenotype as KR-treated or DPP-4 siRNA–transfected 4T1 cells (Supplementary Fig. S1). Also, shRNA-DPP-4–transduced 4T1 cells displayed tumor growth and lung metastasis (Supplementary Fig. S2). We also found that primary tumors in KR-treated mice had a more invasive phenotype, with more metastatic nodules in the lung, as analyzed by H&E staining (Fig. 2C). The coimmunolabeling study with GFP, E-cadherin, and αSMA revealed that 4T1 primary tumors and metastatic lung nodules in KR-treated mice had mesenchymal characteristics (Fig. 2D). Immunoblotting analysis of primary tumor tissues revealed that KR treatment suppressed E-cadherin levels and increased the levels of mesenchymal markers such as αSMA and vimentin (Fig. 2E). Smad3 phosphorylation was induced by KR treatment in primary tumor tissues (Fig. 2F).

DPP-4 suppression promoted CXCL12/CXCR4 axis–induced mTOR pathway activation and EMT

In the presence of KR, CXCL12/CXCR4 expression and mTOR phosphorylation were increased in 4T1 and MDA-MB-231 cells (Fig. 3A and B). This KR-induced induction of CXCL12/CXCR4 expression and mTOR phosphorylation was inhibited by the CXCR4 inhibitor AMD3100 (Fig. 3A and B). KR-induced mTOR phosphorylation was inhibited by rapamycin (Fig. 3C and D).

Next, we investigated the role of the CXCL12/CXCR4/mTOR axis in EMT induced by DPP-4 suppression. Treatment with the KR suppressed E-cadherin and increased αSMA, suggesting the induction of EMT (Fig. 4A and B), similar to the result of the siRNA knockdown experiments in 4T1 and MDA-MB-231 cells (Fig. 1A and B); cotreatment with AMD3100 suppressed KR-induced EMT (Fig. 4A and B). As expected, the mTOR inhibitor rapamycin inhibited KR-induced EMT in both 4T1 and MDA-MB-231 cells (Fig. 4C and D). We performed CXCL12 incubation on the 4T1 cells and found that CXCL12 induced CXCR4 and mTOR activation associated with EMT. Such effects of CXCL12 were enhanced in DPP-4 siRNA–transfected 4T1 cells (Supplementary Fig. S3A). Furthermore, CXCL12-neutralizing antibody reduced DPP-4 siRNA- or KR-induced CXCR4 levels associated with suppression of mTOR activation and EMT (Supplementary Fig. S3B and S3C); CXCL12 cotreatment with AMD3100 or rapamycin suppressed CXCL12 stimulation–induced EMT (Supplementary Fig. S3D and S3E). Transwell assays revealed that KR-mediated suppression of DPP-4 increased the migration of both 4T1 cells and MDA-MB-231 cells compared with control cells (Fig. 4E); this effect on migration was suppressed by either AMD3100 or rapamycin (Fig. 4E). KR-induced EMT was confirmed by gene expression analysis of Snail, Slug, and ZEB1, key molecules for the induction of EMT; AMD3100 and rapamycin suppressed the expression of these EMT-associated proteins in 4T1 cells (Supplementary Fig. S4).

The TGFβ pathway did not contribute to EMT induced by DPP-4 inhibition

TGFβ signaling is a vital player in EMT (21). To understand the role of the interaction between DPP-4 and TGFβ/Smad signaling in EMT, we investigated the levels of TGFβ receptors and downstream signaling molecules. Western blot analysis revealed that DPP-4 knockdown induced TGFβ receptor (TGFβR) 1 and

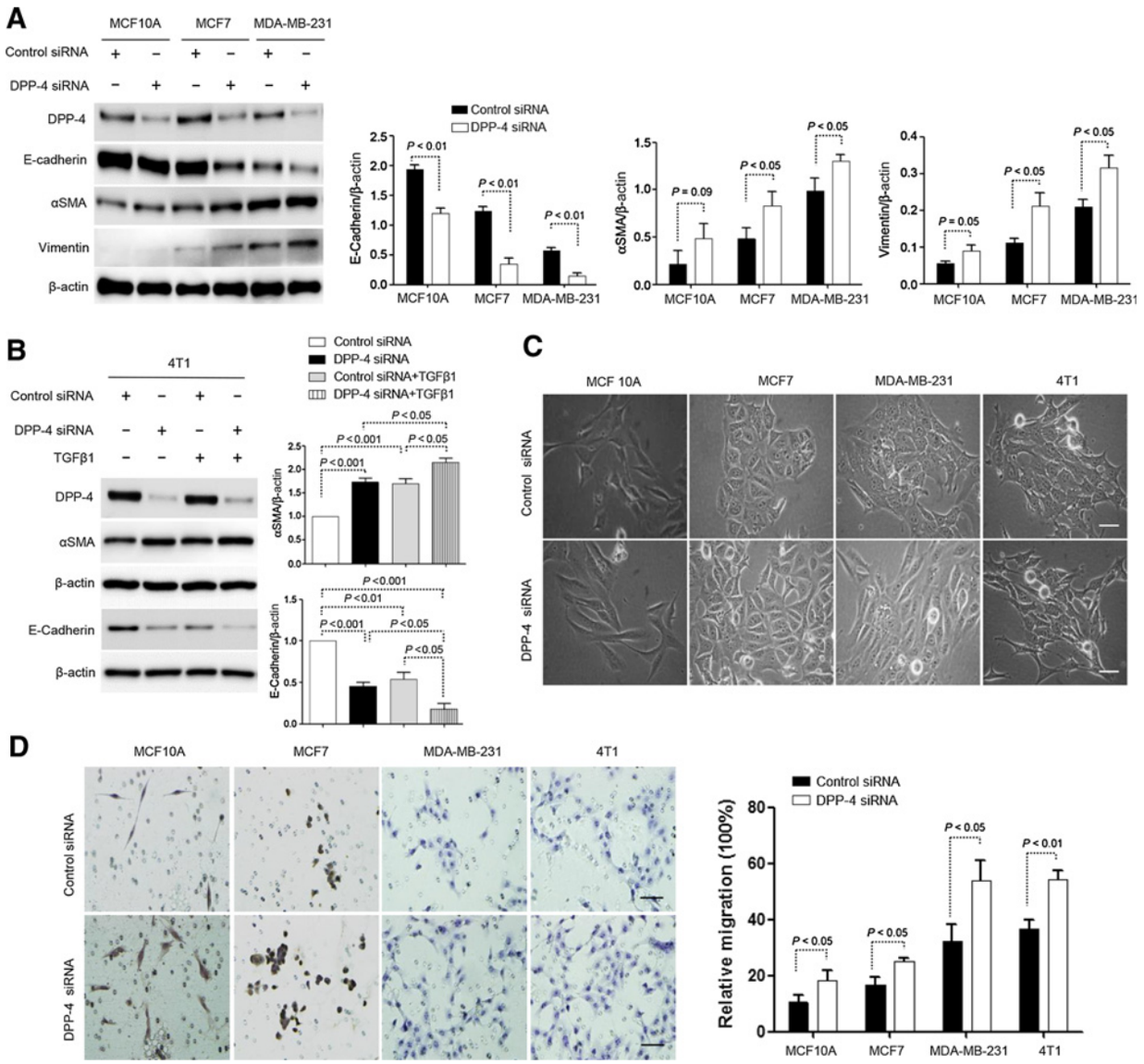

Figure 1.

Silencing DPP-4 promotes EMT in normal mammary epithelial cells and cancer cells. **A,** Western blot analysis of DPP-4, E-cadherin, αSMA, and vimentin in MCF 10A, MCF7, and MDA-MB-231 cells treated for 48 hours in the presence or absence of DPP-4 siRNA (100 nmol/L). Densitometric analysis of protein expression relative to β-actin levels ($n = 3$ per group). **B,** Western blot analysis of DPP-4, E-cadherin, and αSMA. 4T1 cells were treated with or without TGFβ1 (5 ng/mL) for 48 hours in the presence or absence of DPP-4 siRNA (100 nmol/L). Densitometric analysis of each protein level normalized to β-actin levels ($n = 3$ per group). **C,** Morphologic evaluation of MCF 10A, MCF7, MDA-MB-231, and 4T1 cells treated with or without DPP-4 siRNA (100 nmol/L). Six different fields of view were analyzed for each cell group. Images were obtained by microscopy at ×200 magnification (scale bar, 50 μm). **D,** Transwell migration assays in MCF 10A, MCF7, MDA-MB-231, and 4T1 cells transfected with or without DPP-4 siRNA (100 nmol/L) for 48 hours. The cells that migrated through the membrane were stained with hematoxylin and counted in 6 different fields of view. The cell migration data was normalized by cell proliferations as relative cell migration rate = migrated cell number/(post treated cell number−primary cell number) × 100%. Migration images were obtained by microscopy at ×200 magnification (scale bar, 100 μm). The data in the graph are presented as the mean ± SEM.

TGFβR2 expression, and Smad3 phosphorylation in 4T1 cells (Fig. 5A). Similarly, DPP-4 knockdown induced Smad3 phosphorylation in MCF 10A normal breast epithelial cells as well as in both breast cancer cells, MCF7 and MDA-MB-231, yet Smad3 phosphorylation levels were associated with the aggressiveness of cancer cells (Fig. 5B). We also confirmed Western blot analysis of TGFβ1, TGFβ2, TGFβ3, and BMP2, 4. Basically, TGFβ1 was dominantly induced by DPP-4 inhibition (Supplementary Fig. S5). Confocal immunofluorescence images revealed that KR-induced suppression of E-cadherin expression was associated with increased nuclear localization of phosphorylated Smad3 compared with control (Fig. 5C).

To confirm the role of TGFβ signaling in KR-induced EMT, we suppressed TGFβ signaling with a TGFβ-neutralizing antibody

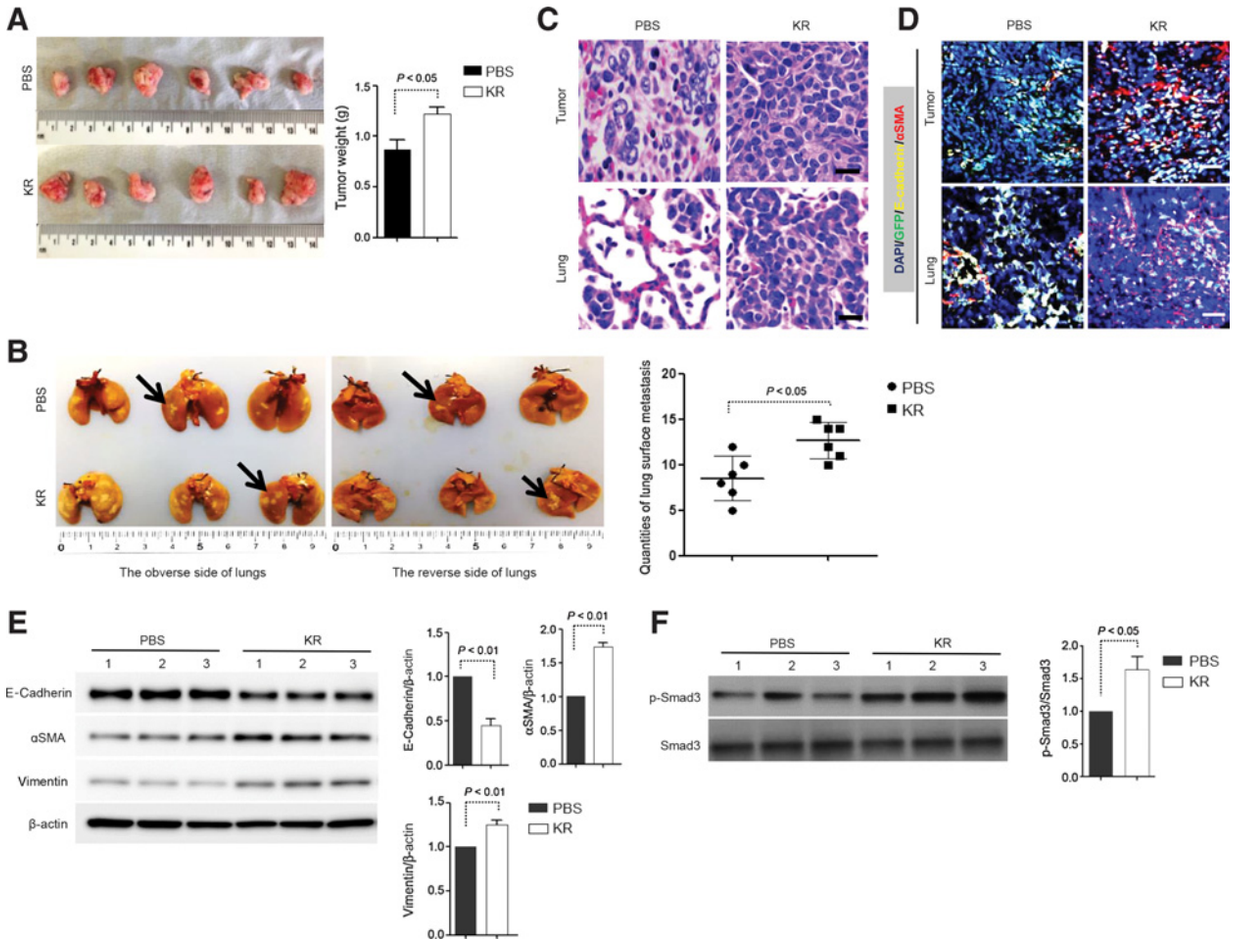

Figure 2.

DPP-4 inhibition promotes EMT and metastasis in orthotopic allograft breast cancer models. **A** and **B,** Representative images of primary tumor (**A**) and lung (**B**) tissues. The 4T1 tumor–bearing female BALB/c mice were treated with PBS or KR62436 (KR, 0.02 mg/g/day, orally); 7 days after treatment was initiated, the mice were sacrificed, and the primary tumors and lungs were removed. The primary tumor weight was determined ($n = 6$), and lung surface metastases, including those on the obverse and reverse sides ($n = 3$), were imaged and quantified. The data in the graph are presented as the mean ± SEM. Black arrows, lung surface metastases. **C,** Representative images of primary tumor and lung sections stained with H&E (scale bar, 25 μm; magnification, ×200). **D,** Representative images of Opal staining for GFP, E-cadherin, and αSMA in primary tumor and lung sections (scale bar, 100 μm; magnification, ×200). **E** and **F,** Western blot analysis of E-cadherin, αSMA, vimentin (**E**), and p-Smad3 (**F**) in primary tumor tissues. Densitometric analysis of protein expression relative to β-actin or Smad3 levels. Representative data from three independent analyses are shown.

(N-TGFβ). N-TGFβ nearly completely suppressed Smad3 phosphorylation (Fig. 5D), but KR-induced EMT was not inhibited by cotreatment with N-TGFβ (Fig. 5D). Moreover, KR-induced expression of CXCL12 and CXCR4 and phosphorylation of mTOR were not suppressed by N-TGFβ (Fig. 5E). However, TGFβR induction and Smad3 phosphorylation by KR were suppressed by AMD3100 (Supplementary Fig. S6).

CXCR4 suppression inhibited KR-induced breast cancer metastasis

Finally, to confirm whether CXCL12/CXCR4 axis plays a critical role in DPP-4 suppression–induced cancer metastasis, we performed AMD3100 intervention study in KR-treated 4T1 tumor–bearing mouse. Compared with PBS-treated mice, DPP-4 activity in all primary tumor, lung, and plasma was suppressed markedly in either KR or KR with AMD3100-treated mice (Fig. 6A). As expected, KR treatment increased the level of CXCL12 in the primary tumor, lung, or plasma (Fig. 6B). Compared with KR treatment alone, KR with AMD3100 inhibited body weight reduction during the course of the experiment (Fig. 6C). MTT assay revealed that AMD3100 suppressed KR-induced proliferation of 4T1 cells (Fig. 6D). AMD3100 treatment also reduced volume (Fig. 6E), weight (Fig. 6F), and invasive phenotype of primary tumor (Fig. 6G) in KR-treated mice. Furthermore, AMD3100 inhibited KR-induced lung metastasis (Fig. 6H and I). The Opal triple immunolabeling revealed that either in primary tumor or lung metastasis, AMD3100 suppressed KR-induced EMT in 4T1 cells that was labelled by GFP (Fig. 6J and K). IHC analysis of primary tumor indicated that KR-treated mice exhibited higher levels of the expression of CXCR4 and mTOR phosphorylation; AMD3100 blocked the KR-induced CXCR4 and mTOR phosphorylation (Fig. 6L). AMD3100 also

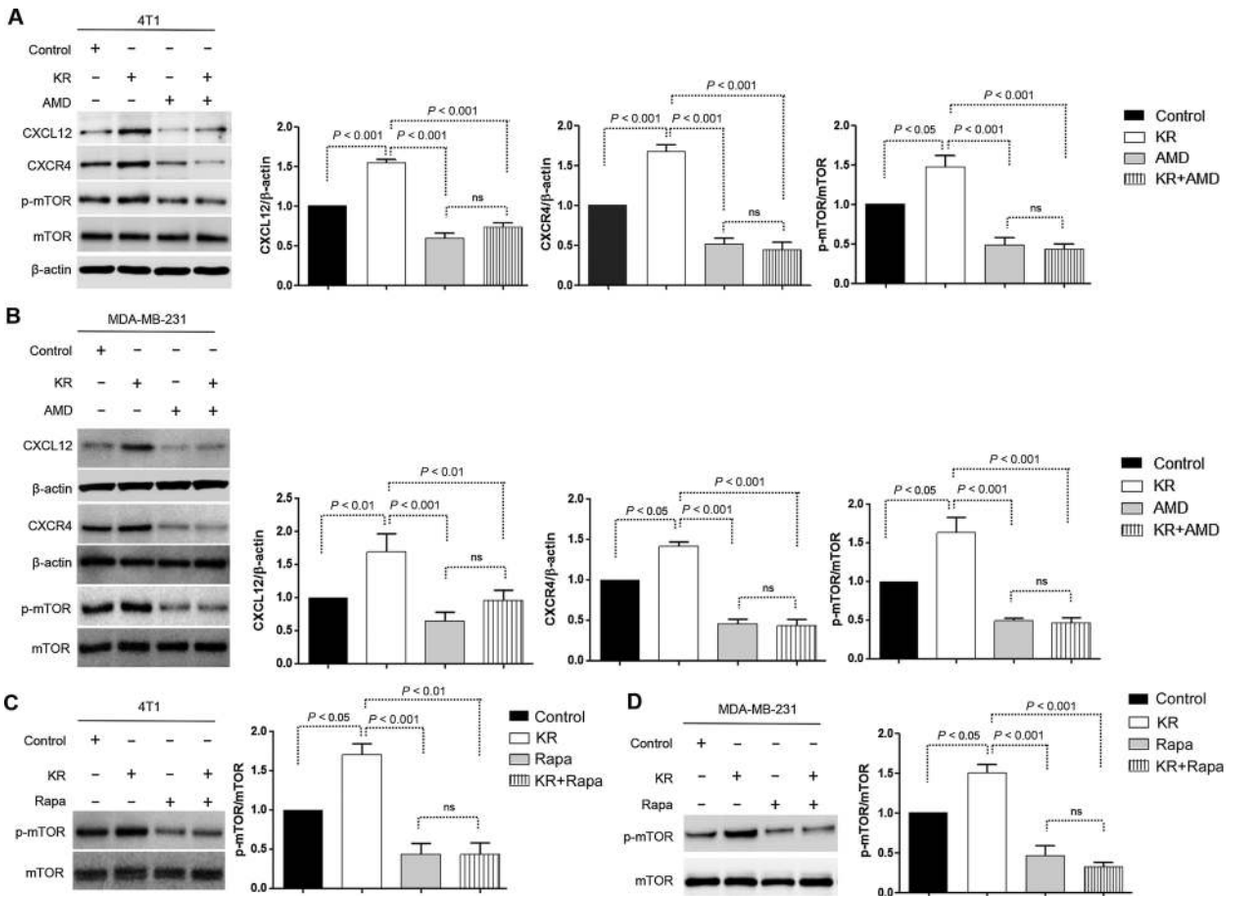

Figure 3.

Inhibition of DPP-4 by KR62436 promotes CXCL12/CXCR4 axis–induced phosphorylation of mTOR. **A** and **B,** Western blot analysis of CXCL12, CXCR4, and p-mTOR in 4T1 (**A**) and MDA-MB-231 (**B**) cells treated with KR62436 (KR, 50 μmol/L), AMD3100 (AMD, 30 μmol/L), or KR and AMD for 48 hours. Densitometric analysis of protein expression relative to β-actin or mTOR levels ($n = 3$ per group). **C** and **D,** Western blot analysis of p-mTOR in 4T1 (**C**) and MDA-MB-231 (**D**) cells treated with KR 62436 (KR, 50 μmol/L), rapamycin (Rapa, 1 μmol/L), or KR and rapamycin for 48 hours. Densitometric analysis of protein expression relative to mTOR levels ($n = 3$ per group).

suppressed the EMT-associated gene expression of Snail, Slug, and ZEB1 in primary tumor tissues (Supplementary Fig. S7).

Discussion

Patients with diabetes have a higher incidence of cancer than the general population, and some antidiabetes drugs could be relevant for the biology of cancer in the context of diabetes (22). Therefore, establishing the safety and potential detrimental effects of diabetes drugs in terms of carcinogenesis and cancer biology is essential for diabetes research. In this study, we focused on the pleiotropic effects of DPP-4 inhibitors, which are in general thought to be beneficial for human health, to better understand the pathologic significance of DPP-4 inhibitors in cancer biology. In brief, we report the following findings: (i) DPP-4 suppression by siRNA, shRNA, or an inhibitor induced EMT in human and mouse breast cancer cells. This induction was more significant in aggressive cancer cells such as 4T1 and MDA-MB-231 cells. (ii) The DPP-4 inhibition increased expression of both CXCL12 and its receptor CXCR4 and phosphorylation of the downstream signaling molecule mTOR. (iii) The CXCR4 inhibitor AMD3100 and the mTOR inhibitor rapamycin each abolished the induction of EMT by DPP-4 suppression. (iv) Unexpectedly, EMT induced by the DPP-4 inhibitor was independent of TGFβ signaling. (v) *In vivo*, the DPP-4 inhibition enhanced the metastasis of 4T1 breast cancer allografts to the lung in a CXCL12/CXCR4–dependent manner. These data provide clear evidence that DPP-4 negatively regulates cancer metastasis via cleavage of CXCL12, and that a DPP-4 inhibitor could potentially facilitate this endogenous metastasis mechanism in patients with cancer.

Currently, it remains unclear whether DPP-4 inhibitors are detrimental to patients with diabetes with existing tumors. In general, patients with cancer are excluded from drug development and clinical trial of diabetes therapies. Furthermore, the notion that metastasis in patients with cancer could be associated with a prescribed drug is rarely considered. Wang and colleagues reported that the DPP-4 inhibitors saxagliptin and sitagliptin increased the migration and invasion of multiple cancer cell lines through nuclear factor E2–related factor 2 (NRF2) in a KEAP1-C151–dependent manner (23). In our analysis of the molecular mechanism by which DPP-4 inhibition promotes cancer metastasis, we focused on DPP-4 biology in chemokine processing.

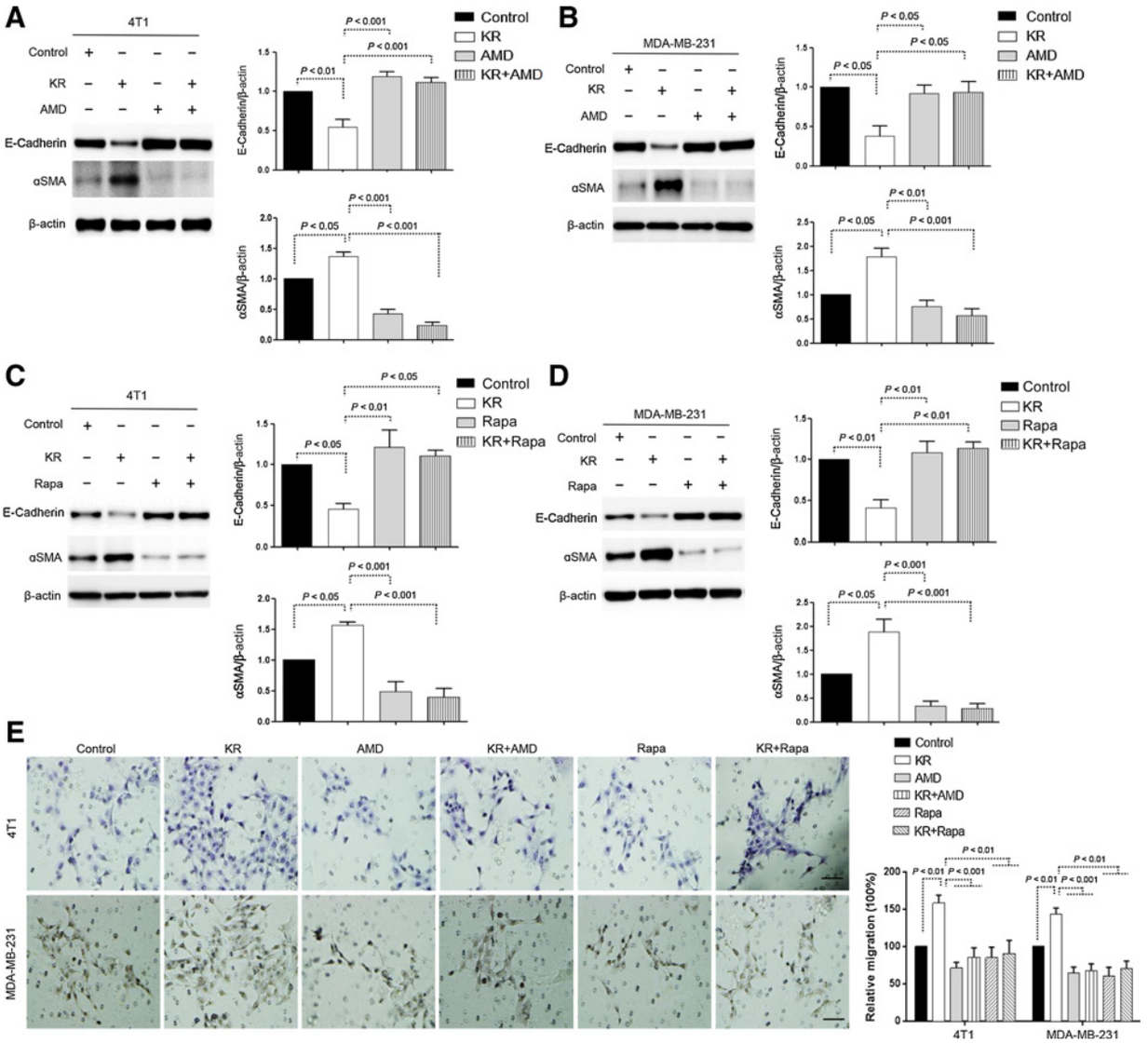

Figure 4.

AMD3100 or rapamycin blocks the KR62436-induced mesenchymal and invasive phenotype in metastatic cell lines. **A** and **B,** Western blot analysis of E-cadherin and αSMA in 4T1 (**A**) and MDA-MB-231 (**B**) cells treated with KR62436 (KR, 50 μmol/L), AMD3100 (AMD, 30 μmol/L), or KR and AMD for 48 hours. Densitometric analysis of protein expression relative to β-actin levels ($n = 3$ per group). **C** and **D,** Western blot analysis of E-cadherin and αSMA in 4T1 (**C**) and MDA-MB-231 (**D**) cells treated with KR62436 (KR, 50 μmol/L), rapamycin (Rapa, 1 μmol/L), or KR and rapamycin for 48 hours. Densitometric analysis of protein expression relative to β-actin levels ($n = 3$ per group). **E,** Transwell assays in 4T1 and MDA-MB-231 cells treated with KR62436 (KR, 50 μmol/L), AMD3100 (AMD,30 μmol/L), KR and AMD, rapamycin (Rapa, 1 μmol/L), KR and AMD, or KR and rapamycin for 48 hours. The cells that migrated through the membrane were counted in 6 different fields of view. The cell migration data was normalized by cell proliferations as relative cell migration rate = migrated cell number/(post treated cell number−primary cell number) × 100%. Migration images were obtained by microscopy at ×200 magnification (scale bar, 100 μm). The data in the graph are presented as the mean ± SEM.

DPP-4 cleaves a number of chemokines and cytokines, such as CXCL12, GM-CSF and granulocyte colony-stimulating factor (G-CSF; ref. 24). CXCL12 is inactivated by exopeptidases, such as DPP-4, matrix metalloproteinase (MMP)-2, and MMP-9 (24). CXCL12 and its specific receptor CXCR4 play important roles in hematopoiesis, angiogenesis, stem cell homing, and tumor development and behavior (25). Furthermore, a recent report showed that disruption of mTORC1 is sufficient to decrease cell proliferation and CXCR4-mediated migration in HeLa cells, and blockade of mTORC1 by rapamycin decreases primary tumor growth and CXCR4-mediated lymph node metastasis and increases animal survival (26). Evidence has shown that mTOR knockdown in SW480 colon cancer cells increases E-cadherin levels and decreases vimentin and αSMA levels (27). The results we present here indicate that DPP-4 suppression induces the CXCL12/CXCR4 axis and the subsequent activation of mTOR, which are associated with the induction of EMT. Interestingly, these pathways could underlie a beneficial effect of DPP-4

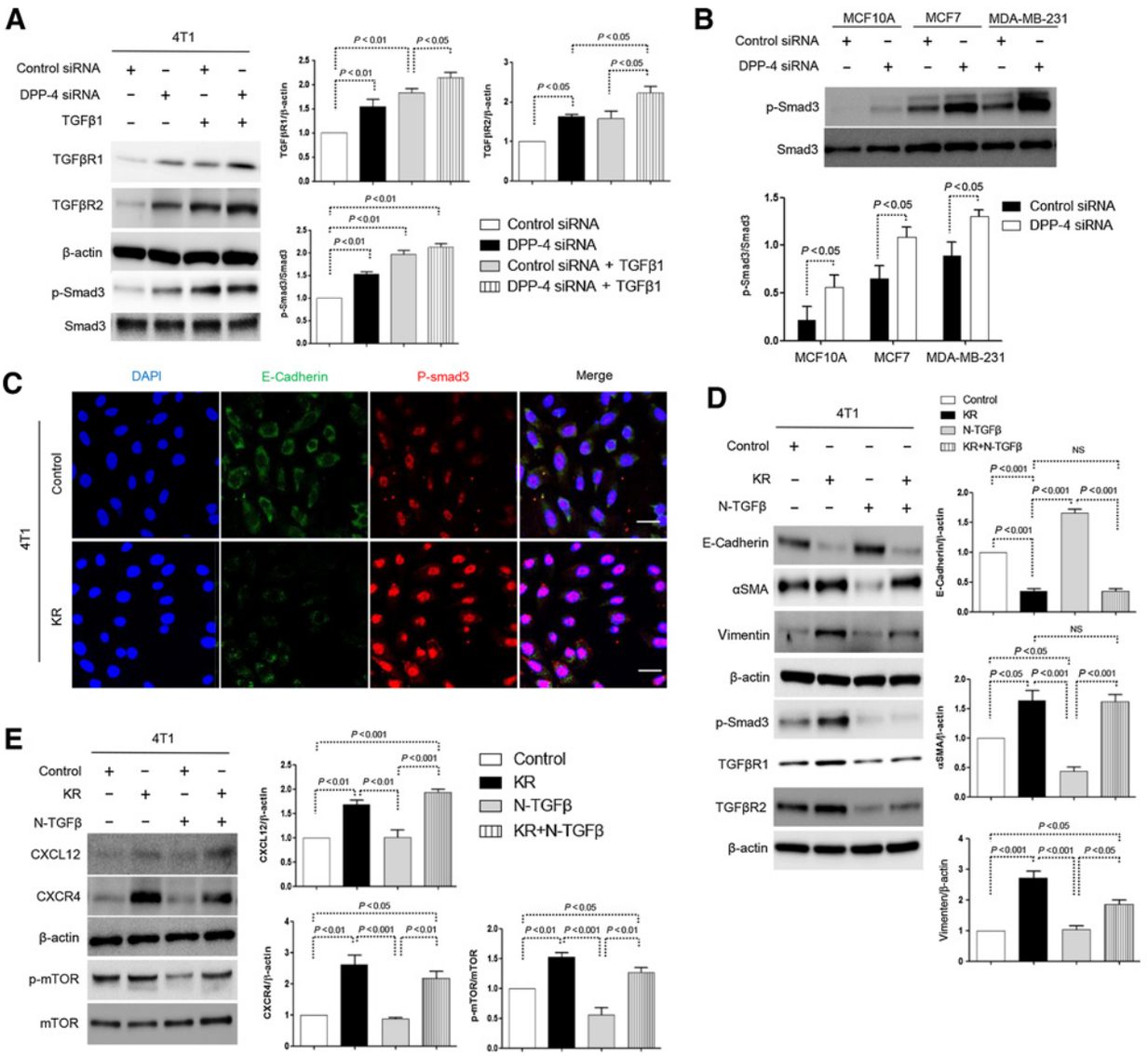

Figure 5.

DPP-4 inhibition promotes EMT in a TGFβ signal–independent manner. **A,** Western blot analysis of TGFβR1, TGFβR2, and p-Smad3 in DPP-4 siRNA–transfected 4T1 cells. The cells were treated with TGFβ1 (5 ng/mL) for 48 hours in the presence or absence of DPP-4 siRNA (100 nmol/L). Densitometric analysis of protein expression relative to β-actin or Smad3 levels is shown ($n = 3$ per group). **B,** Western blot analysis of p-Smad3 in DPP-4 siRNA–transfected MCF 10A, MCF7, and MDA-MB-231 cells. Densitometric analysis of each protein normalized to Smad3 ($n = 3$ per group). **C,** Immunocytofluorescence analysis of E-cadherin and p-Smad3 coexpression in 4T1 cells following KR62436 (KR, 50 μmol/L) treatment for 48 hours. For each slide, representative images of six different fields of view at ×200 magnification were evaluated. The scale bar indicates 100 μm in each panel. **D** and **E,** Western blot analysis of E-cadherin, αSMA, vimentin, p-Smad3, TGFβR1, TGFβR2, CXCL12, CXCR4, and p-mTOR in 4T1 cells treated with KR62436 (KR,50 μmol/L), neutralizing TGFβ (1, 2, 3) antibody (N-TGFβ, 1.0 μg/mL), or KR and N-TGFβ for 48 hours. Densitometric analysis of protein expression relative to β-actin levels ($n = 3$ per group).

inhibitors in terms of wound healing in patients with diabetes (28). The effects of DPP-4 on CXCL12 cleavage are well known; the data suggest that these effects of DPP-4 inhibitors on CXCR4-positive cancer cells are potentially universal for any DPP-4 inhibitors.

Epithelial cells and endothelial cells can transform into mesenchymal cells in response to certain types of stress or insults (29). Indeed, we have shown that DPP-4 suppression in endothelial cells represses TGFβ2–induced EndMT (30–32). Such effects of DPP-4 inhibition are thought to associate with the induction of antifibrotic miRs such as let-7 and miR-29, which have been shown to inhibit TGFβ signaling (33). In contrast, surprisingly, our findings revealed that DPP-4 suppression is sufficient to induce EMT and cell migration in normal mammary epithelial cells and cancer cells. With regard to this, DPP-4 inhibition increased TGFβ/Smad signaling in breast cancer, but neutralization of TGFβ had absolutely no effect on the induction of EMT by DPP-4

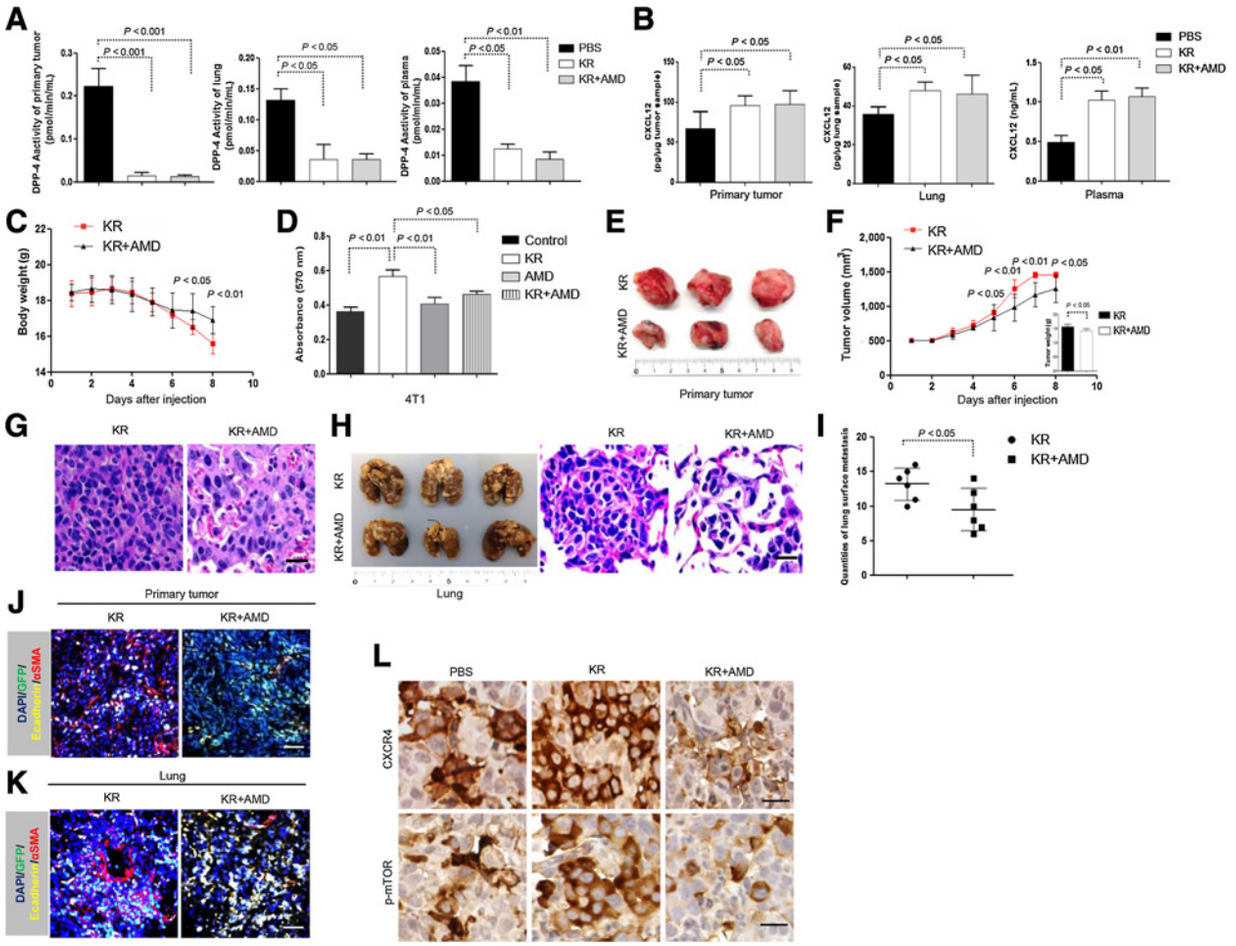

Figure 6.

AMD3100 suppresses breast cancer metastasis in KR62436-treated tumor-bearing mice. **A** and **B,** The analysis of DPP-4 activity (**A**) and CXCL12 quantity (**B**) in primary tumor, lung, and plasma of 4T1 tumor–bearing female BALB/c mice treated with PBS, KR62436 (KR, 0.02 mg/g/day, orally), or KR and AMD3100(AMD, 0.0075 mg/g/day i.p.) for 7 days. The data in the graphs are shown as mean ± SEM; $n = 6$. **C,** The analysis of body weight of 4T1 tumor–bearing female BALB/c mice. The mouse breast cancer models were treated with KR62436 (KR, 0.02 mg/g/day, orally) or KR and AMD3100 (AMD, 0.0075 mg/g/day i.p.) for 7 days. The data in the curve graph are expressed as mean ± SEM. $n = 6$. **D,** MTT assay of 4T1 cells treated with KR62436 (KR, 50 μmol/L), AMD3100 (AMD, 30 μmol/L), or KR and AMD for 48 hours. The absorbance is shown as mean ± SEM; $n = 3$. **E,** Representative images of primary tumor tissue. **F,** The tumor volume in each group was measured ever day during the medicine intervention, and the tumor weight (bottom right) in each group was detected after sacrifice. The data in the graphs are shown as mean ± SEM; $n = 6$. **G,** Tumor sections were stained with H&E in each group. H&E images at ×200 magnification were obtained by microscopy. Scale bars, 25 μm. **H** and **I,** The lung surface metastases (**H**) were imaged and the quantification of lung metastases (**I**) was performed. The lung sections were stained with H&E in each group (**H**). H&E images at ×200 magnification were obtained by microscopy. Scale bars, 25 μm. The data in the graphs are shown as mean ± SEM; $n = 3$. **J** and **K,** Representative images of Opal staining for GFP, E-cadherin, and αSMA in primary tumor (**J**) and lung (**K**) sections. Scale bars, 100 μm. Magnification, ×200. **L,** The IHC analysis of CXCR4 and p-mTOR in PBS, KR62436 (KR, 0.02 mg/g/day, orally), or KR- and AMD3100 (AMD, 0.0075 mg/g/day i.p.)-treated mice. The images at ×400 magnification were obtained by NanoZoomer Digital Pathology System. Scale bars, 10 μm.

inhibition. This DPP-4 inhibitor–stimulated TGFβ signaling pathway was dependent on CXCL12/CXCR4 in breast cancer cells. Furthermore, inhibiting DPP-4 in TGFβ-treated cells further stimulated the induction of EMT. These data suggest that the effects of DPP-4 inhibition on mesenchymal transformation of either epithelial cells or endothelial cells could rely on cell type and the degree of dependence on the TGFβ signaling pathway.

Recently, studies have confirmed that there is cross-talk between the TGFβ and CXCL12 pathways. Evidence indicates that TGFβ induces CXCR4 in tumor cells (34), enhancing the response to CXCL12 to promote invasion and metastasis (35). We also revealed that DPP-4 suppression induces TGFβ/Smad signaling, but the TGFβ-induced CXCR4 cascade was not relevant for DPP-4–induced EMT and metastasis because the KR-induced CXCL12/CXCR4/mTOR axis and EMT were not suppressed by the TGFβ-neutralizing antibody. These findings further confirm that KR-induced EMT via the CXCL12/CXCR4/mTOR axis is independent of TGFβ/Smad signaling. The role of TGFβ/Smad signaling–dependent CXCL12/CXCR4 pathway activation by DPP-4 suppression in cancer biology is not clear, and further study is absolutely needed.

In conclusion, we show here that DPP-4 inhibition accelerates breast cancer metastasis by inducing EMT through CXCL12/CXCR4–mediated mTOR activation. These data indicate that DPP-4 inhibitors, in general thought to be safe, could be harmful in a select population of patients with CXCR4-positive cancer. Further study is necessary to monitor the effects of DPP-4 inhibitors on human tumorigenesis. Moreover, these biological characteristics of DPP-4 in cancer cells could lead to the identification of novel therapeutic targets for cancer.

Disclosure of Potential Conflicts of Interest

K. Kanasaki is a consultant/advisory board member for Japan Boehringer Ingelheim and Japan Eli Lilly and reports receiving speakers' bureau honoraria from Japan Eli Lilly, Japan Boehringer Ingelheim, Tanabe Mitsubishi, Ono Pharmaceutical, Novartis, and Takeda Pharmaceutical Company. No potential conflicts of interest were disclosed by the other authors.

Authors' Contributions

Conception and design: F. Yang, Y. Takagaki
Development of methodology: F. Yang, Y. Takagaki, J. Li, K. Kanasaki
Acquisition of data (provided animals, acquired and managed patients, provided facilities, etc.): Y. Takagaki, T. Ikeda, A. Kumagai, E. Kawakita
Analysis and interpretation of data (e.g., statistical analysis, biostatistics, computational analysis): F. Yang
Writing, review, and/or revision of the manuscript: F. Yang, A. Kumagai
Administrative, technical, or material support (i.e., reporting or organizing data, constructing databases): Y. Takagaki, Y. Yoshitomi, J. Li, M. Kitada, S. Shi
Study supervision: K. Kanasaki, D. Koya
Others (discussion of data): M. Kitada

Acknowledgments

This work was partially supported by grants from the Japan Society for the Promotion of Science (23790381 and 26460403 to K. Kanasaki; 25282028 and 25670414 to D. Koya), a grant for Collaborative Research (C2011-4 and C2012-1 to D. Koya), a grant for Promoted Research (S2016-3 and S2017-1 to K. Kanasaki), a grant for Assist KAKEN (K2017-16 to Y. Takagaki) from Kanazawa Medical University, and Lilly-Incretin Basic Research Grant from the Japan Diabetes Foundation (to Y. Takagaki). F. Yang is supported by the Japanese Government MEXT (Ministry of Education, Culture, Sports, Science, and Technology) Fellowship Program (142309) and S. Shi is supported by foreign scholar grants from Kanazawa Medical University. Boehringer Ingelheim (Japan), Mitsubishi Tanabe Pharma, and Ono Pharmaceutical contributed to establishing the Division of Anticipatory Molecular Food Science and Technology. K. Kanasaki is under a consultancy agreement with Boehringer Ingelheim.

The costs of publication of this article were defrayed in part by the payment of page charges. This article must therefore be hereby marked *advertisement* in accordance with 18 U.S.C. Section 1734 solely to indicate this fact.

Received February 26, 2018; revised September 21, 2018; accepted December 13, 2018; published first December 24, 2018.

References

1. Heerboth S, Housman G, Leary M, Longacre M, Byler S, Lapinska K, et al. EMT and tumor metastasis. Clin Transl Med 2015;4:6.
2. Ghoncheh M, Pournamdar Z, Salehiniya H. Incidence and mortality and epidemiology of breast cancer in the World. Asian Pac J Cancer Prev 2016;17:43–6.
3. Tohme S, Simmons RL, Tsung A. Surgery for cancer: a trigger for metastases. Cancer Res 2017;77:1548–52.
4. Wu Y, Zhou BP. New insights of epithelial-mesenchymal transition in cancer metastasis. Acta Biochim Biophys Sin 2008;40:643–50.
5. Nieto MA, Huang RY, Jackson RA, Thiery JP. Emt: 2016. Cell 2016;166:21–45.
6. Tomaskovic-Crook E, Thompson EW, Thiery JP. Epithelial to mesenchymal transition and breast cancer. Breast Cancer Res 2009;11:213.
7. Bae EJ. DPP-4 inhibitors in diabetic complications: role of DPP-4 beyond glucose control. Arch Pharm Res 2016;39:1114–28.
8. Gokhale M, Buse JB, Gray CL, Pate V, Marquis MA, Sturmer T. Dipeptidyl-peptidase-4 inhibitors and pancreatic cancer: a cohort study. Diabetes Obes Metab 2014;16:1247–56.
9. Amritha CA, Kumaravelu P, Chellathai DD. Evaluation of anti cancer effects of DPP-4 inhibitors in colon cancer- an *in vitro* study. J Clin Diagn Res 2015;9:FC14–6.
10. Nagel AK, Ahmed-Sarwar N, Werner PM, Cipriano GC, Van Manen RP, Brown JE. Dipeptidyl peptidase-4 inhibitor-associated pancreatic carcinoma: a review of the FAERS database. Ann Pharmacother 2016;50:27–31.
11. Amin S, Boffetta P, Lucas AL. The role of common pharmaceutical agents on the prevention and treatment of pancreatic cancer. Gut Liver 2016;10:665–71.
12. Metzemaekers M, Van Damme J, Mortier A, Proost P. Regulation of chemokine activity - a focus on the role of dipeptidyl peptidase IV/CD26. Front Immunol 2016;7:483.
13. Christopherson KW II, Frank RR, Jagan S, Paganessi LA, Gregory SA, Fung HC. CD26 protease inhibition improves functional response of unfractionated cord blood, bone marrow, and mobilized peripheral blood cells to CXCL12/SDF-1. Exp Hematol 2012;40:945–52.
14. Mego M, Cholujova D, Minarik G, Sedlackova T, Gronesova P, Karaba M, et al. CXCR4-SDF-1 interaction potentially mediates trafficking of circulating tumor cells in primary breast cancer. BMC Cancer 2016;16:127.
15. Hernandez L, Magalhaes MA, Coniglio SJ, Condeelis JS, Segall JE. Opposing roles of CXCR4 and CXCR7 in breast cancer metastasis. Breast Cancer Res 2011;13:R128.
16. Mortier A, Gouwy M, Van Damme J, Proost P, Struyf S. CD26/dipeptidylpeptidase IV-chemokine interactions: double-edged regulation of inflammation and tumor biology. J Leukoc Biol 2016;99:955–69.
17. Engelman JA. Targeting PI3K signalling in cancer: opportunities, challenges and limitations. Nat Rev Cancer 2009;9:550–62.
18. Bracho-Valdes I, Moreno-Alvarez P, Valencia-Martinez I, Robles-Molina E, Chavez-Vargas L, Vazquez-Prado J. mTORC1- and mTORC2-interacting proteins keep their multifunctional partners focused. IUBMB Life 2011;63:896–914.
19. Chang LH, Chen CH, Huang DY, Pai HC, Pan SL, Teng CM. Thrombin induces expression of twist and cell motility via the hypoxia-inducible factor-1alpha translational pathway in colorectal cancer cells. J Cell Physiol 2011;226:1060–8.
20. Chen G, Chen SM, Wang X, Ding XF, Ding J, Meng LH. Inhibition of chemokine (CXC motif) ligand 12/chemokine (CXC motif) receptor 4 axis (CXCL12/CXCR4)-mediated cell migration by targeting mammalian target of rapamycin (mTOR) pathway in human gastric carcinoma cells. J Biol Chem 2012;287:12132–41.
21. Nagaraj NS, Datta PK. Targeting the transforming growth factor-beta signaling pathway in human cancer. Expert Opin Investig Drugs 2010;19:77–91.
22. Sen S, He Y, Koya D, Kanasaki K. Cancer biology in diabetes. J Diabetes Investig 2014;5:251–64.
23. Wang H, Liu X, Long M, Huang Y, Zhang L, Zhang R, et al. NRF2 activation by antioxidant antidiabetic agents accelerates tumor metastasis. Sci Transl Med 2016;8:334ra51.
24. Zillessen P, Celner J, Kretschmann A, Pfeifer A, Racke K, Mayer P. Metabolic role of dipeptidyl peptidase 4 (DPP4) in primary human (pre)adipocytes. Sci Rep 2016;6:23074.
25. Xu C, Zhao H, Chen H, Yao Q. CXCR4 in breast cancer: oncogenic role and therapeutic targeting. Drug Des Devel Ther 2015;9:4953–64.
26. Delgado-Martin C, Escribano C, Pablos JL, Riol-Blanco L, Rodriguez-Fernandez JL. Chemokine CXCL12 uses CXCR4 and a signaling core formed by bifunctional Akt, extracellular signal-regulated kinase (ERK) 1/2, and mammalian target of rapamycin complex 1 (mTORC1) proteins

to control chemotaxis and survival simultaneously in mature dendritic cells. J Biol Chem 2011;286:37222–36.
27. Pandurangan AK. Potential targets for prevention of colorectal cancer: a focus on PI3K/Akt/mTOR and Wnt pathways. Asian Pac J Cancer Prev 2013;14:2201–5.
28. Long M, Cai L, Li W, Zhang L, Guo S, Zhang R, et al. DPP-4 inhibitors improve diabetic wound healing via direct and indirect promotion of epithelial-mesenchymal transition and reduction of scarring. Diabetes 2018;67:518–31.
29. Zhu XY, Urbieta-Caceres V, Krier JD, Textor SC, Lerman A, Lerman LO. Mesenchymal stem cells and endothelial progenitor cells decrease renal injury in experimental swine renal artery stenosis through different mechanisms. Stem Cells 2013;31:117–25.
30. Kanasaki K, Konishi K, Hayashi R, Shiroeda H, Nomura T, Nakagawa A, et al. Three ileus cases associated with the use of dipeptidyl peptidase-4 inhibitors in diabetic patients. J Diabetes Investig 2013;4: 673–5.
31. Kanasaki K. The pathological significance of dipeptidyl peptidase-4 in endothelial cell homeostasis and kidney fibrosis. Diabetoly Int 2016;7:212–20.
32. Shi S, Kanasaki K, Koya D. Linagliptin but not Sitagliptin inhibited transforming growth factor-beta2-induced endothelial DPP-4 activity and the endothelial-mesenchymal transition. Biochem Biophys Res Commun 2016;471:184–90.
33. Srivastava SP, Shi S, Kanasaki M, Nagai T, Kitada M, He J, et al. Effect of antifibrotic MicroRNAs crosstalk on the action of N-acetyl-seryl-aspartyl-lysyl-proline in diabetes-related kidney fibrosis. Sci Rep 2016;6: 29884.
34. Zhao XP, Huang YY, Huang Y, Lei P, Peng JL, Wu S, et al. Transforming growth factor-beta1 upregulates the expression of CXC chemokine receptor 4 (CXCR4) in human breast cancer MCF-7 cells. Acta Pharmacol Sin 2010;31:347–54.
35. Smith HA, Kang Y. The metastasis-promoting roles of tumor-associated immune cells. J Mol Med 2013;91:411–29.